RSC Advances

This is an *Accepted Manuscript*, which has been through the Royal Society of Chemistry peer review process and has been accepted for publication.

Accepted Manuscripts are published online shortly after acceptance, before technical editing, formatting and proof reading. Using this free service, authors can make their results available to the community, in citable form, before we publish the edited article. This *Accepted Manuscript* will be replaced by the edited, formatted and paginated article as soon as this is available.

You can find more information about *Accepted Manuscripts* in the Information for Authors.

Please note that technical editing may introduce minor changes to the text and/or graphics, which may alter content. The journal's standard Terms & Conditions and the Ethical guidelines still apply. In no event shall the Royal Society of Chemistry be held responsible for any errors or omissions in this *Accepted Manuscript* or any consequences arising from the use of any information it contains.

ROYAL SOCIETY OF CHEMISTRY

www.rsc.org/advances

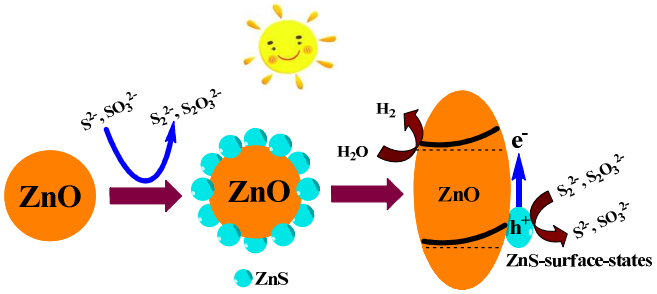

Light-assisted preparation of a ZnS/ZnO nanocomposite for efficiently visible-light driven H_2 evolution from water

RSC Advances Accepted Manuscript

Cite this: DOI: 10.1039/c0xx00000x

www.rsc.org/xxxxxx

ARTICLE TYPE

Facile preparation of a ZnS/ZnO nanocomposite for robust sunlight photocatalytic H_2 evolution from water

Hui Zhao, Yuming Dong,* Pingping Jiang,* Xiuming Wu, Ruixian Wu, and Yanmei Chen

Received (in XXX, XXX) Xth XXXXXXXXX 20XX, Accepted Xth XXXXXXXXX 20XX

DOI: 10.1039/b000000x

A ZnS/ZnO nanocomposite was facilely and cost-effectively prepared for visible light photocatalytic H_2 evolution. ZnS/ZnO showed good H_2 evolution activity (187 μmol $g^{-1}h^{-1}$) and stability (nearly linear H_2 production rate even after 16 h) without any co-catalyst. Furthermore, ZnS/ZnO revealed superior catalytic performance in sunlight-driven H_2 evolution (1807 μmol $g^{-1}h^{-1}$). Due to the electronic hybridization of ZnO band structures with ZnS-surface-states, the band bending and surface dipole moment of ZnO could occur. Under visible-light irradiation, the electrons at the ZnO-ZnS interfaces can be excited from the bent valence bend level induced to the conduction bend of ZnO for water reduction, while the holes trapped by ZnS-surface-states can be quenched by the sacrificial reagent (S^{2-}/SO_3^{2-}). The created ZnS-ZnO interfaces with ZnS-surface-states led to a lower band gap energy and enabled the visible light response.

Introduction

Increasing awareness of the importance of energy crisis and environmental pollution has stimulated great progress in the development of green renewable energy. Hydrogen is regarded as a potential fuel for renewable energy. Photocatalytic water decomposition into hydrogen is a valuable approach to utilize solar energy, which is recognized as a green and promising way to produce clean energy and solve the fossil fuel shortage problem and environmental issues.[1,2] In recent years, visible light photocatalytic hydrogen generation from water by using semiconductor materials has attracted increasing attention.[3-6] In spite of these intensive achievements, developing robust, stable and inexpensive photocatalysts for water splitting remains a serious challenge within the field.

As important II-VI semiconductors, ZnO and ZnS contain only earth-abundant elements and have been intensively studied in a wide range of UV sensors, lasers, field emitters, nanogenerators, solar cells, photocatalysis, etc.[7] Unfortunately, both ZnO and ZnS had a large band gap (Eg = 3.37 and 3.67 eV for ZnO and ZnS, respectively), and thus there is almost no adsorption in the visible light region, which largely limits their application in visible-light-driven water splitting. Recently, the heterostructures of ZnO and ZnS have attracted theoretical and experimental interest because the combination of these two wide bandgap semiconductors can yield a novel material with the photoexcitation threshold energy lower than the individual components, leading to improved physical and chemical properties.[8,9] According to our knowledge, apart from ZnS/ZnO hybrid nanowires,[10] few literature was reported on ZnS/ZnO nanocomposites used as effective catalysts for visible light photocatalytic hydrogen production. The preparation of reported ZnS/ZnO hybrid nanowires was conducted by a high-temperature hydrothermal method involving the use of expensive, toxic and smelly 16-mercaptohexadecanoic acid, which makes it difficult to be scaled up and does serious harm to environmental protection and people's health. Therefore, new preparation strategy of ZnS/ZnO heterostructure is greatly desirable to make the best use of ZnO and ZnS for solar energy application.

Herein, a ZnS/ZnO nanocomposite is easily prepared by the photodeposition of ZnS on the surface of ZnO nanoparticles in photocatalytic process, and ZnO nanoparticls can be abundantly and conveniently obtained by a facile precipitation-anneal method using inexpensive and nontoxic inorganic salt and ammonium hydroxide as raw materials. The ZnS/ZnO revealed good catalytic activity and stability in visible-light-driven water splitting and natural sunlight-driven hydrogen evolution.

Experimental section

Preparation

The ZnS/ZnO nanocomposite is formed in photocatalytic hydrogen production process using ZnO nanoparticles as raw materials. To obtain ZnO nanoparticles, 20 mL of 6.0 mol/L aqueous ammonia was slowly added into 150 mL of 0.01 mol/L $Zn(CH_3COO)_2$ aqueous solution. After stirring for 3 days, the resulting precipitates were separated, washed, dried and annealed at 500 ^oC (Supplementary Fig. S1).

Characterization

X-ray diffraction (XRD) patterns were recorded on a D8 X-ray diffractometer (Bruker AXS, German) to identify the composition and phase of sample. Transmission electron microscopy (TEM) image was collected on a JEM-2100 transmission electron

RSC Advances Accepted Manuscript

microscope (JEOL, Japan) to examine the morphology and size of sample. Energy-dispersive X-ray spectroscopy (EDX) was taken on the TEM. Raman spectra were recorded on a confocal microscopic Raman spectrometer (Renishow In-Via) with a 785 nm laser light irradiation from 100 to 700 cm^{-1} at a duration time of 10 s. To detect surface species of sample, X-ray photoelectron spectroscopy (XPS) analysis was conducted using an ESCALAB 250 Xi (Thermo, USA) X-ray photoelectron spectrometer with Al Kα line as the excitation source (hν = 1484.6 eV) and adventitious carbon (284.6 eV for binding energy) was used as reference to correct the binding energy of sample. The photoluminescence (PL) spectra of the photocatalyst were measured on a Cary Esclipse spectrometer (Varian, USA) with an excitation wavelength of 325 nm. Inductively coupled plasma atomic emission spectrometer (ICP-AES, Leeman Prodigy, USA) was used to detect the element content in the sample.

Photocatalytic hydrogen production

The photocatalytic experiments were performed in a 37 mL flask at ambient temperature using a 300 W Xe lamp equipped with UV cut off filter (λ > 400 nm). 10 mg of ZnO was added in an aqueous solution (total volume = 10 mL) containing 0.45 M Na_2S and 0.45 M Na_2SO_3, and then the suspension was stirred for 15 min in the dark. Before each experiment, the suspension was purged with gas mixture of nitrogen and methane (Vnitrogen : Vmethane = 4 : 1) for 40 min to remove air. Methane served as the internal standard. Hydrogen gas evolution was measured by gas chromatography (SP-6890, nitrogen as a carrier gas) with a thermal conductivity detector (TCD).

Photoelectrochemical Measurement

A working electrode was prepared as follows: 20 mg of sample was dispersed in 4 mL water. 150 μL of the resultant suspension was uniformly droped onto a 1×1 cm^2 indium-tin oxide glass (ITO glass) and then dried at 70 ℃ for 1 h to obtain the working electrodes. Photocurrents were measured on a CHI600D electrochemical analyzer (Chenhua Instruments Co. Shanghai) in a standard three-electrode system by using the prepared electrode as the working electrode, a Pt net as the counter electrode, and Ag/AgCl as the reference electrode. A 300W Xe-lamp equipped with a band-glass light filter (> 400 nm) served as a light source. The electrolyte was a buffer solution (pH=6) containing 0.30 mol/L hexamethylenetetramine and 0.10 mol/L hydrochloric acid.

Results and discussion

In this work, ZnS/ZnO nanocomposite was formed by the photodeposition of ZnS on the surface of ZnO in photocatalytic H_2 production process. When light was bombarded on the surface of ZnO, the holes and electrons generated (Eqs. 1). The surface of ZnO underwent dissolution in alkaline sulfide solution for the formation of ZnS on the surface of ZnO particles.[11] Na_2S + Na_2SO_3 solution acted as a hole scavenger by three possible routes (Eqs. 2, 3 and 4).[12-14] The production of S_2^{2-} ions (Eqs. 3) efficiently reacted with SO_3^{2-} ions (Eqs. 5) with the generation of $S_2O_3^{2-}$ and S^{2-}.[15] In the presence of H^+, $S_2O_3^{2-}$ ions (Eqs. 4 and 5) transformed to HSO_3^{2-} ions and S (Eqs. 6). Finally, it became a fact that the formation of ZnS on the surface of ZnO appeared to occur (Eqs. 7 and 8) in the aqueous Na_2S + Na_2SO_3 solution with photoirradiation.

$$ZnO + h\nu \rightarrow ZnO\ (e_{CB}^- + h_{VB}^+)\ (1)$$
$$SO_3^{2-} + H_2O + 2\ h_{VB}^+ \rightarrow SO_4^{2-} + 2H^+\ (2)$$
$$2S^{2-} + 2\ h_{VB}^+ \rightarrow S_2^{2-}\ (3)$$
$$SO_3^{2-} + S^{2-} + 2\ h_{VB}^+ \rightarrow S_2O_3^{2-}\ (4)$$
$$S_2^{2-} + SO_3^{2-} \rightarrow S_2O_3^{2-} + S^{2-}\ (5)$$
$$S_2O_3^{2-} + H^+ \rightarrow HSO_3^- + S\ (6)$$
$$Zn^{2+} + S^{2-} \rightarrow ZnS\ (7)$$
$$Zn^{2+} + S + 2e^- \rightarrow ZnS\ (8)$$

Fig.1a showed XRD patterns of ZnO and ZnS/ZnO. ZnO displayed the characteristic XRD peaks corresponding to (100), (002), (101), (102), (110), (103), (202), (112) and (201) reflections of wurtzite ZnO (JCPDS No.36-1451). Diffraction peaks related to impurity was not observed. For ZnS/ZnO, new XRD peaks indexed to (111), (220) and (311) planes of wurtzite ZnS (JCPDS No.05-0566) appeared, which indicated that ZnS formed on the surface of ZnO. The decreased peak intensity of ZnO in ZnS/ZnO illustrated that the formation of ZnS tended to low the crystallization of ZnO. Fig.1b presented Raman spectra of ZnO and ZnS/ZnO. A typical Raman band was located at 437 cm^{-1} for ZnO, which corresponded to the E2 (high) vibrational mode implying the existence of the wurtzite structure.16 At the same time, there are three new Raman bands at 153, 260 and 342 cm^{-1} for ZnS/ZnO. The two Raman bands at 342 cm^{-1} and 260 cm^{-1} matched the corresponding longitudinal (LO) and transverse (TO) phonon modes of wurtzite ZnS while the Raman band at 153 cm^{-1} was caused by the small size of the as-synthesized ZnS.[17,18] Similarly, in comparison with ZnO, the decreased Raman band intensity of ZnO was observed for ZnS/ZnO.

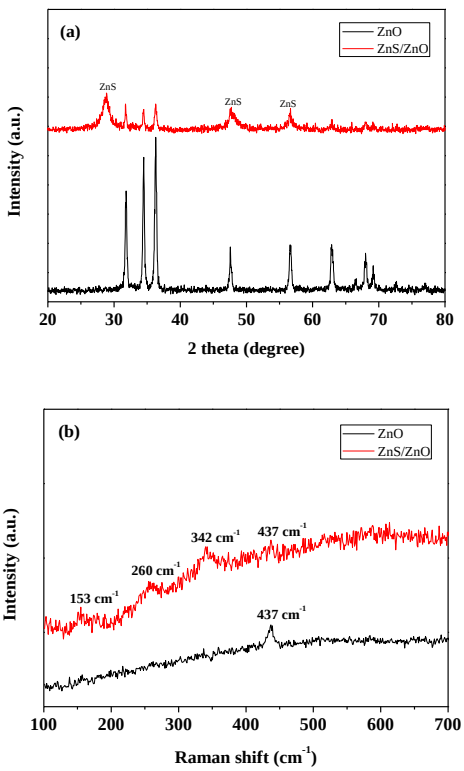

Fig. 1 XRD patterns (a) and Raman spectra (b) of ZnO and ZnS/ZnO.

RSC Advances Accepted Manuscript

This journal is © The Royal Society of Chemistry [year]

Fig. 2a presented the TEM micrograph of ZnO. It was clearly observed that the size of ZnO nanoparticles was about 50~80 nm. For ZnS/ZnO nanocomposite, the generated ZnS particles with small size of ca. 5~10 nm accumulated on ZnO surface, as shown in Fig. 2b. Fig. 2c demonstrated a representative high-resolution TEM micrograph of ZnS/ZnO. The lattice fringes with the spacing of 0.25 nm and 0.31 nm were in good agreement with the interplanar spacing of the (101) plane of wurtzite ZnO and the interplanar spacing of the (111) plane of wurtzite ZnS, respectively. Fig. 2d gave the EDX spectrum of ZnS/ZnO. The Zn, O and S were obviously observed and the total atomic percents of O and S were similar to that of Zn, further indicating the ZnS/ZnO composite structure.

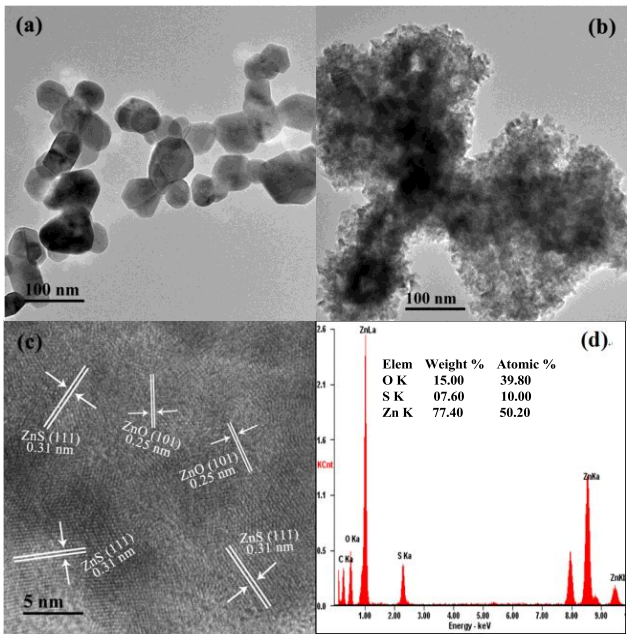

Fig. 2 TEM images of ZnO (a) and in-situ ZnS/ZnO (b), HRTEM (c) image and EDX spectrum (d) of ZnS/ZnO.

Fig. 3 gave XPS analysis results of ZnS/ZnO. Fig. 3a showed the scan survey spectra for the representative ZnS/ZnO. All of the peaks on the curve can be ascribed to Zn, O, S and C elements. The presence of C element mainly came from the hydrocarbon contaminants that commonly existed for XPS. Therefore, it can be concluded that the sample was composed of Zn, O and S only, which was consistent with the XRD results. The position of Zn 2p3/2 and Zn 2p5/2 peaks for the sample (Fig. 3b) were at about 1021.1 eV and 1044.2 eV, which confirmed that Zn element existed mainly in the form of Zn^{2+} chemical state on the sample surface. Fig. 3c showed the O 1s peak for ZnS/ZnO, which can be fitted into two peaks. The lower energy peak located at 531.0 eV corresponded to the oxygen atoms coordinated with Zn atoms, while the higher energy peak centered at 532.5 eV can be ascribed to the oxygen adsorbed on ZnS/ZnO surface. The position of the S 2p peak (Fig. 3d) was at about 161.0 eV, which confirmed that S element existed mainly in the form of S^{2-} chemical state on the sample surface.

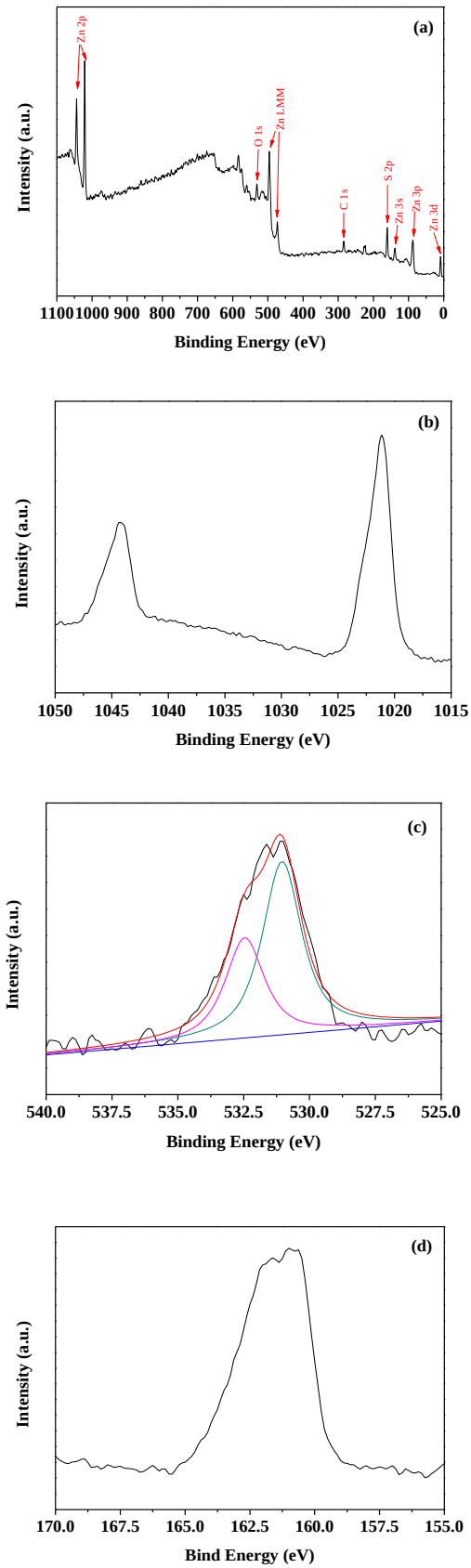

Fig. 3 (a) Survey scan XPS spectra in the binding energy range 0~1100 eV and high-resolution spectra, (b) Zn 2p, (c) O1s, (d) S 2p of ZnS/ZnO.

RSC Advances Accepted Manuscript

Fig. 4a showed the photocatalytic activity of ZnS/ZnO for H_2 generation under visible light irradiation ($\lambda > 400$ nm). H_2 production enhanced with the increase of irradiation time. During 2 h, the corresponding H_2 evolution was 374 μmol g^{-1}, which was higher than that of the reported materials.[10,19] The results illustrated that the prepared ZnS/ZnO was an efficient catalyst for photocatalytic H_2 evolution from water. In addition, the effects of different Na_2S/Na_2SO_3 concentrations were investigated and the results were given in Fig. 4b. The photocatalytic H_2 production first increased with an increase in the Na_2S and Na_2SO_3 concentration. Generally, a certain increase of Na_2S/Na_2SO_3 concentration could be expected for the better diffusion of the reacting species to the surface of photocatalysts. However, a decrease in the H_2 evolution was found with further increase of Na_2S and Na_2SO_3 concentration. There existed an optimal concentration of 0.45 mol/L Na_2S/0.45 mol/L Na_2SO_3 for H_2 evolution. Obviously, the H_2 evolution rate was more sensitive to S^{2-} anion in comparison with SO_3^{2-}. Since Na_2S and Na_2SO_3 played an important role in formation of ZnS/ZnO, it is very necessary to investigate the effects of different Na_2S/Na_2SO_3 concentrations on the ratio of ZnS to ZnO, especially for the effect of Na_2S due to its high responsibility to photocatalytic H_2 evolution. The contents of ZnS in ZnS/ZnO composites under different Na_2S concentrations were summarized in Table 1. As the Na_2S concentration increased from 0.15 to 0.45 M, the weight percent of ZnS increased from 16.58% to 20.70%. Obviously, an increase amount of ZnS-surface-states formed, and thereby led to the increasing photocatalytic H_2 evolution activity. Meanwhile, it was well known that a certain increase of Na_2S concentration as a hole scavenger could be expected for the better diffusion of the reacting species to the surface of photocatalysts subsequently causing the enhance of photocatalytic H_2 ecolution activity. However, with the further increase of Na_2S concentration to 0.55 M, the weight percent of ZnS reached to 21.83%. In this way, although more rich ZnS-surface-states existed, the photocatalytic H_2 evolution slightly decreased. According to previously reported literature,[15,20] the largest H_2 evolution can not be obtained in the presence of concentrated Na_2S as a hole scavenger. This possibly explained the decreasing photocatalytic H_2 activity for ZnS/ZnO with more rich ZnS-surface-states at the condition of 0.55 M Na_2S used.

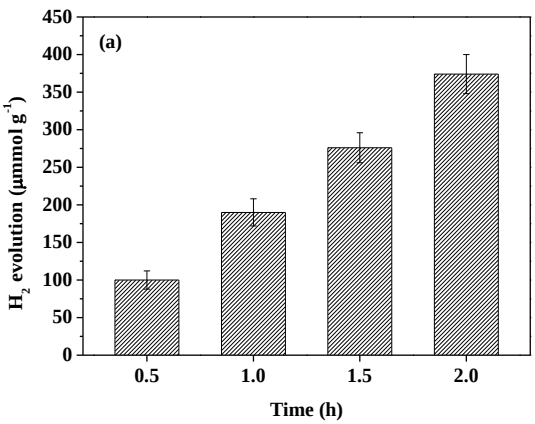

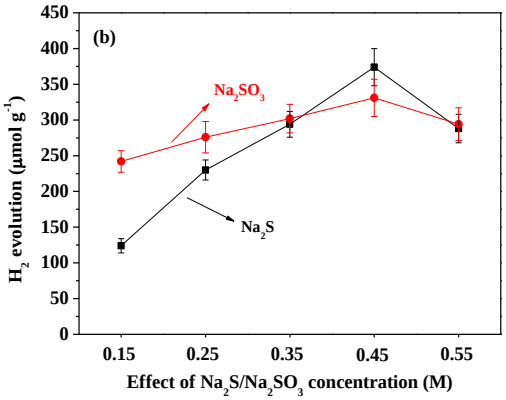

Fig. 4 (a) Photocatalytic hydrogen production during 2 h in a 10 mL aqueous solution containing 0.45 M Na_2S and 0.45 M Na_2SO_3 suspended with 10 mg of ZnO under visible light irradiation ($\lambda > 400$ nm); (b) Effect of Na_2S/Na_2SO_3 concentration on the photocatalytic hydrogen production during 2 h in a 10 mL aqueous solution containing 0.45 M Na_2SO_3/0.25 M Na_2S suspended with 10 mg of ZnO under visible light irradiation ($\lambda >$ 400 nm)

Table 1 Content of S for ZnS/ZnO under different Na_2S concentrations determined by ICP-AES

Samples	Na_2S concentration (M)	S (wt%)	ZnS (wt%)
ZnS/ZnO[a]	0.15	5.47	16.58
ZnS/ZnO[b]	0.25	5.95	18.04
ZnS/ZnO[c]	0.35	6.48	19.64
ZnS/ZnO[d]	0.45	6.83	20.70
ZnS/ZnO[e]	0.55	7.20	21.83

The weight percent of ZnS was calculated by the content of S.

In view of practical applications, besides catalytic activity, the stability and durability are also indispensable to photocatalysts. In order to evaluate the stability of ZnS/ZnO, we performed the long time curse of H_2 evolution experiment under visible light. Fig. 5 presented the H_2 evolution as the function of irradiation time. The H_2 production was nearly linear even after 16 h of irradiation without renewing the sacrificial agents, and more than 2112 μmol g^{-1} H_2 was produced during the course of the 16 h experiment, indicating the good stability of the ZnS/ZnO sample for photocatalytic H_2 production.

RSC Advances Accepted Manuscript

This journal is © The Royal Society of Chemistry [year]

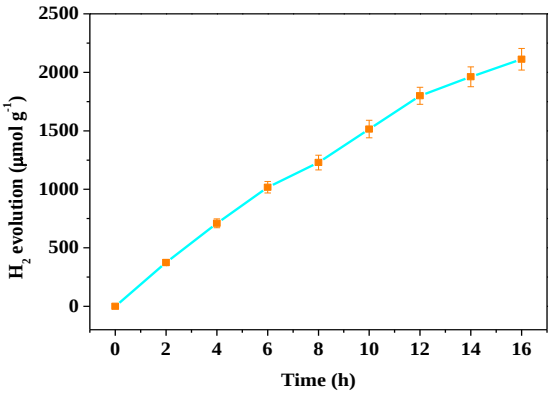

Fig. 5 Photocatalytic hydrogen production in a 10 mL aqueous solution containing 0.45 M Na_2S and 0.45 M Na_2SO_3 suspended with 10 mg of ZnO under visible light irradiation ($\lambda > 400$ nm).

The ultimate goal of photocatalyst is high-efficiency application of sunlight and solar energy. Therefore, H_2 evolution was also conducted under direct sunlight outdoors (Supplementary Fig. S2). As shown in Fig. 6, H_2 production increased with the prolongation of sunlight irradiation time. During 2 h, H_2 evolution reached 3580 μmol g^{-1}, which was nearly 10 times higher than that under visible light irradiation from Xe lamp. When the sunlight irradiation time prolonged to 4 h, the corresponding H_2 production increased to 7230 μmol g^{-1}. These results indicated that ZnS/ZnO was a robust catalyst for sunlight-driven H_2 evolution from water. Such heterostructure may be expected to be promising candidates as effective sunlight photocatalyst and potential technological applications.

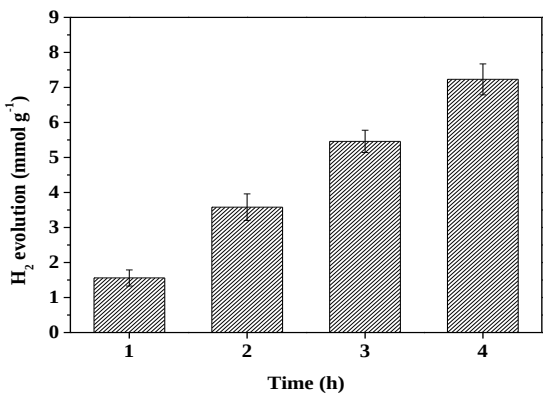

Fig. 6 Photocatalytic hydrogen production during 4h in a 10 mL aqueous solution containing 0.45 M Na_2S and 0.45 M Na_2SO_3 suspended with 0.01 g of ZnO under sunlight irradiation in Wuxi city 2014. Experimental condition: Outdoor temperature: 30 ~ 32 °C, Time: 10: 00 ~ 14: 00.

According to our knowledge, the reported studies on ZnS-ZnO nanocomposites visible light response have revealed that the band alignment can be shifted at the ZnS-ZnO interface for their visible light activities.[21-23] Especially, Lahiri et al. have observed an increase of the work function of ZnO upon the formation of ZnS monolayer on the ZnO surface, which was attributed to band bending and surface dipole moment due to the electronic hybridization of ZnO band structures with the surface states induced by the ZnS monolayer, resulting in an effective band gap of about 2.8 eV for the visible-light excitation.[24]

In our ZnS/ZnO nanocomposite, ZnS particles with size of several nanometers formed on ZnO surface. As shown, the Raman analysis (Fig. 1b) and TEM, HRTEM images (Fig. 2b and 2c) had proved that almost each ZnO nanoparticle was surrounded by many ZnS nanocrystals with directly contacted interfaces. This would create numerous ZnS-surface-states on ZnO nanoparticle surfaces.[24] Due to the electronic hybridization of ZnO band structure with the ZnS-surface-states, the band bending of ZnO occurred.[24] Thus, as illustrated in Fig. 7, it became possible that the electrons at the ZnO-ZnS interfaces could be excited from the bent valence band level to the conduction bend of ZnO which can be applied for water reduction, while the photogenerated holes trapped by ZnS-surface-states would be subjected to quenching by the sacrificial reagent (S^{2-}/SO_3^{2-}). In this way, the effective band gap at the ZnO-ZnS interface would be narrowed, which enabled excitation under visible-light irradiation. The similar results have been reported in photocatalytic H_2 evolution with ZnS-ZnO hybrid nanowires photocatalysts.[10]

In order to prove the visible light response for the as-prepared ZnS/ZnO, the absorption spectra of ZnO and ZnS/ZnO were recorded and shown in Fig 8. The excitonic absorption peak of ZnO was around 355 nm. However, the ZnS/ZnO nanocomposite showed the absorption band at about 380 nm with an absorption edge up to 460 nm, which was red-shifted in comparison with the absorption feature of ZnO. The observation verified that ZnS-surface states on ZnO surface were responsible for the absorption in the visible region. In order to verify the charge transfer mechanism, photoluminescence (PL) emission spectra and photoelectrochemical (PEC) I-t curves were performed to study the charge recombination and transfer behavior of ZnO and ZnS/ZnO as presented in Fig 9. Fig. 9a gave the PL spectra of ZnO and ZnS/ZnO with an excitation wavelength of 325 nm. The emission peak at about 495 nm for ZnO corresponded to the band gap for the recombination of photogenerated electrons and holes.[12] Compared ZnO with ZnS/ZnO, the peak intensity at 495 nm of ZnO obviously decreased due to the presence of ZnS-surface-states enhancing the charge transfer. Figure 9b presented the PEC I-t curves of ZnO and ZnS/ZnO electrodes under intermittent visible light irradiation at -0.22 V vs Ag/AgCl. Compared with ZnO, ZnS/ZnO hybrid photocatalyst showed the higher photocurrent density, which indicated the efficient photogenerated charge transfer between ZnO and ZnS-surface-states for ZnS/ZnO.

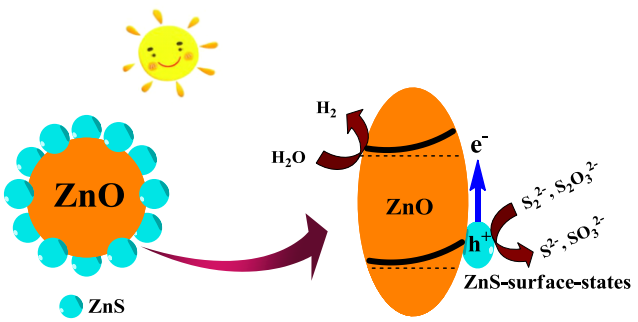

Fig. 7 Graphical representation for the photocatalytic H_2 production.

RSC Advances Accepted Manuscript

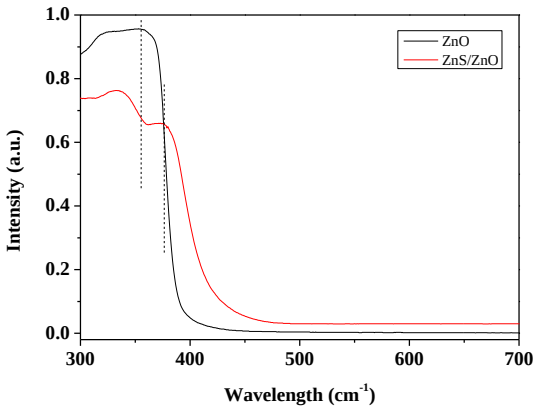

Fig. 8 UV-vis-diffuse reflection spectra of ZnO and ZnS/ZnO.

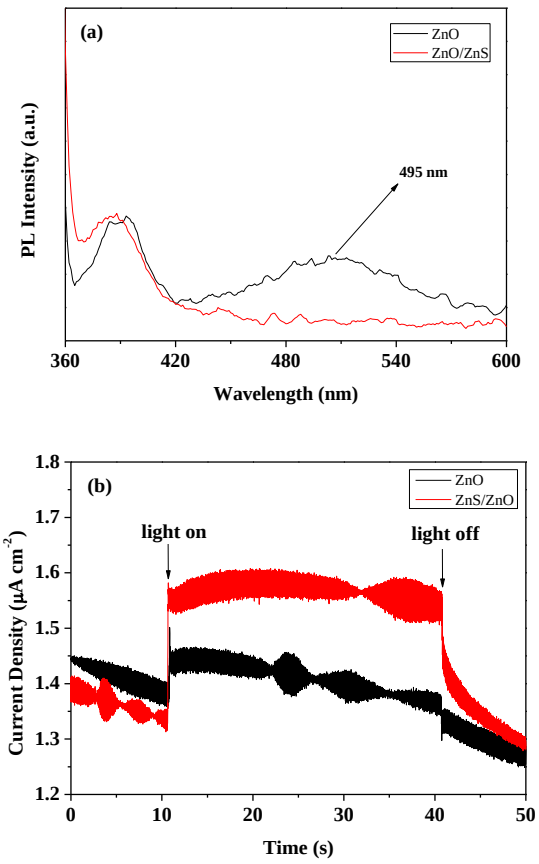

Fig. 9 Comparison of photoluminescence spectra (a) and transient photocurrent responses (I-t) at -0.22 V vs Ag/AgCl (b) of ZnO and ZnS/ZnO.

Conclusions

In conclusion, a novel preparation strategy of ZnS/ZnO heterostructure was designed and realized by the photodeposition of ZnS on the surface of ZnO nanoparticles, while ZnO nanoparticls can be abundantly and conveniently obtained by a facile precipitation-anneal method using inexpensive and nontoxic inorganic salt and ammonium hydroxide as raw materials. ZnS/ZnO showed the good H_2 evolution activity and stability without any co-catalyst under visible light irradiation. Additionally, ZnS/ZnO was confirmed as an efficient catalyst for sunlight-driven H_2 evolution. The electronic hybridization of ZnO band structures with ZnS-surface-states could cause the band bending and surface dipole moment of ZnO. Under visible light irradiation, the electrons at the ZnO-ZnS interfaces could be excited from the bent valence bend level induced to the conduction bend of ZnO for water reduction, while the holes trapped by ZnS-surface-states can be subjected to quenching by the sacrificial reagent (S^{2-}/SO_3^{2-}). The created ZnS-ZnO interfaces with ZnS-surface states led to a lower band gap energy of the composite allowing for the excitation under visible-light irradiation. This work could provide new insights into the facial fabrication of photocatalysts with high performance and facilitate their practical application in solar energy field.

Acknowledgement

The authors gratefully acknowledge the support from the National Natural Science Foundation of China (No. 20903048, 21275065), the Fundamental Research Funds for the Central Universities (JUSRP51314B and JUDCF13015), the Postgraduate Innovation Project of Jiangsu Province (CXZZ13-0743) and MOE & SAFEA for the 111 Project (B13025).

Notes and references

Key Laboratory of Food Colloids and Biotechnology (Ministry of Education of China), School of Chemical and Material Engineering, Jiangnan University, Wuxi 214122, P. R. China. Fax: (+) 86-510-85917763; E-mail: dongym@jiangnan.edu.cn, ppjiang@jiangnan.edu.cn

† Electronic Supplementary Information (ESI) available: [details of any supplementary information available should be included here]. See DOI: 10.1039/b000000x/

1 Q. Wang, J. Li, Y. Bai, J. Lian, H. Huang, Z. Li, Z. Lei, and W. Shangguan, *Green Chem.*, 2014, **16**, 2728-2735.
2 Z. Yan, X. Yu, Y. Zhang, H. Jia, Z. Sun, and P. Du, *Appl. Catal. B: Environ.*, 2014, **160-161**, 173-178.
3 S. R. Lingampalli, U. K. Gautam, and C. N. R. Rao, *Energy Environ. Sci.*, 2013, **6**, 3589-3594.
4 P. Gao, Z. Liu, and D. D. Sun, *J. Mater. Chem. A*, 2013, **1**, 14262-14269.
5 Y. P. Xie, Z. B. Yu, G. Liu, X. L. Ma, and H. M. Cheng, *Energy Environ. Sci.*, 2014, **7**, 1895-1901.
6 X. Wang, L. Yin, and G. Liu, *Chem. Commun.*, 2014, **50**, 3460-3463.
7 X. Huang, M. Wang, L. Shao, M. G. Willinger, C. S. Lee, and X. M. Meng, *J. Phys. Chem. Lett.*, 2013, **4**, 740-744.
8 X. Huang, M. Wang, M. G. Willinger, L. Shao, D. S. Su, and X. M. Meng, *ACS Nano*, 2012, **6**, 7333-7339.
9 W. Chen, H. Ruan, Y. Hu, D. Li, Z. Chen, J. Xian, J. Chen, X. Fu, Y. Shao, and Y. Zheng, *CrystEngComm*, 2012, **14**, 6295-6305.
10 Z. Wang, S. W. Cao, S. C. J. Loo, and C. Xue, *CrystEngComm*, 2013, **15**, 5688-5693.
11 T. Arai, S. Senda, Y. Sato, H. Takahashi, K. Shinoda, B. Jeyadevan, and K. Tohji, *Chem. Mater.*, 2008, **20**, 1997-2000.
12 P. Gomathisankar, K. Hachisuka, H. Katsumata, T. Suzuki, K. Funasaka, and S. Kaneco, *ACS Sustainable Chem. Eng.*, 2013, **1**, 982-988.
13 P. Gomathisankar, K. Hachisuka, H. Katsumata, T. Suzuki, K. Funasaka, and S. Kaneco, *Int. J. Hydrogen Energy*, 2013, **38**, 8625-8630.
14 P. Gomathisankar, K. Hachisuka, H. Katsumata, T. Suzuki, K. Funasaka, and S. Kaneco, *RSC Adv.*, 2013, **3**, 20429-20436.
15 N. Bao, L. Shen, T. Takata, and K. Domen, *Chem. Mater.*, 2008, **20**, 110-117.

RSC Advances Accepted Manuscript

This journal is © The Royal Society of Chemistry [year]

16 A. P. Bhirud, S. D. Sathaye, R. P. Waichal, L. K. Nikama, and B. B. Kale, *Green Chem.*, 2012, **14**, 2790-2798.
17 C. Lan, K. Hong, W. Wang, and G. Wang, *Solid State Commun.*, 2003, **125**, 455-458.
18 Q. Wu, H. Cao, S. Zhang, X. Zhang, and D. Rabinovich, *Inorg. Chem.*, 2006, **45**, 7316-7322.
19 H. Zhou, L. Ding, T. Fana, J. Ding, D. Zhang, and Q. Guo, *Appl. Catal. B: Environ.*, 2014, **147**, 221-228.
20 Z. Yan, Ha. Wu, A. Han, X. Yu, and P. Du, *Int. J. Hydrogen Energy*, 2014, **39**, 13353-13360.
21 Y. Hu, H. Qian, Y. Liu, G. Du, F. Zhang, L. Wang and X. Hu, *CrystEngComm*, 2011, 13, 3438-3443.
22 J. Schrier, D. O. Demchenko and L. W. Wang, *Nano Lett.*, 2007, 7, 2377-2382.
23 Z. Wang, J. Wang, T.-K. Sham and S. Yang, *J. Phys. Chem. C*, 2012, 116, 10375-10381.
24 J. Lahiri, and M. Batzill, *J. Phys. Chem. C*, 2008, **112**, 4304-4307.

RSC Advances Accepted Manuscript